Predation, evo-devo, and historical contingency: A nematode predator drives evolution of aggregative multicellularity

Running title: Evolution of an aggregative mesopredator

Kaitlin A. Schaal[1,2,*], Marco La Fortezza[2], Lok Man Yuen[2], & Gregory J. Velicer[2]

[1]Department of Evolution, Ecology & Behaviour, University of Liverpool, Liverpool, UK; [2]Institute of Integrative Biology, ETH Zürich, Zürich, Switzerland

* Corresponding author. Email: contact@kaitlinschaal.com

Marco La Fortezza: marco.lafortezza@env.ethz.ch
Lucina Yuen: lucina.yuen@env.ethz.ch
Gregory J. Velicer: gregory.velicer@env.ethz.ch

Competing Interests: The authors declare no competing interests.

Authorship statement: KAS and GJV designed the evolution experiment. KAS, MLF, and GJV designed the fruiting body morphological analysis. KAS carried out the experimental work, except for the time lapse experiment. KAS, MLF, LMY, and GJV designed the time lapse experiment; LMY carried it out; LMY and MLF analyzed it. KAS performed the remaining statistical analysis. MLF advised on the statistical analysis. KAS, MLF, and GJV wrote the paper. KAS, MLF, LMY, and GJV revised the paper.

Acknowledgements: We thank Hinrich Schulenburg, Ralf Sommer, and Peter Zee for advice and discussion. Some strains were provided by the CGC, which is funded by NIH Office of Research Infrastructure Programs (P40 OD010440). This research was supported in part by an EMBO Long-Term Fellowship (ALTF 1208–2017) to M.L.F. and in part by Swiss National Science Foundation (SNSF) grants 31003A_16005 and 310030B_182830 to G.J.V.

Predation, evo-devo, and historical contingency: A nematode predator drives evolution of aggregative multicellularity

Running title: Evolution of an aggregative mesopredator

Major article

Keywords:

evolution of multicellularity, food webs, mesopredator, microbial evolutionary ecology, *Myxococcus*, predator-prey interactions

Words in manuscript: 8431

Elements of manuscript:

Abstract

Introduction

Methods

Results (including figures)

Discussion

Literature cited

Supplemental Information (separate document)

Abstract. Regulated aggregation and differentiation of cells is an intriguing form of multicellularity that produces diverse morphological forms, resulting from an interplay of complex evolutionary, regulatory, behavioral, and social mechanisms. We investigate the potential for predation to shape aggregative multicellularity evolution across different combinations of three species comprising a multi-trophic food web. The bacterium *Myxococcus xanthus*, which can develop into spore-filled fruiting bodies, is a mesopredator; the bacterivorous nematode *Pristionchus pacificus* is an apex predator, and the bacterium *Escherichia coli* is a shared basal prey for both predators. The number and morphology of *M. xanthus* fruiting bodies responds evolutionarily to nematodes, regardless of whether *E. coli* is present. *E. coli* alone with *M. xanthus* reduces both fruiting body formation and spore production, but the presence of nematodes eliminates those effects. *M. xanthus* lineages with an ancestral antibiotic resistance mutation evolved less overall, revealing strong historical contingency and suggesting potential tradeoffs between antibiotic resistance and responsiveness to biotic selection. Our results suggest that predation both of and by mesopredators has played important roles in the evolution of aggregative multicellularity and reveal complex inter-trophic evolutionary interactions in a relatively simple three-species food web.

Introduction

The advent of clonal multicellularity (CM) is a Major Evolutionary Transition and is much studied (Stanley 1973; Bonner 1998; Ratcliff et al. 2012; Pentz et al. 2015; Herron 2016; Herron et al. 2022), but less attention has been given to understanding the origins, diversity, and evolutionary drivers of aggregative multicellularity (AM). Through AM, microbial cells that live independently for part of their life cycle come together to engage in and benefit from group behaviors. AM emerged multiple times, in both prokaryotes and eukaryotes, yet understanding of its evolutionary origins and what selective factors drive its diversification – potentially including being subject to predation – remains poor (Pentz et al. 2020; La Fortezza and Velicer 2021; Márquez-Zacarías et al. 2021; Herron et al. 2022; La Fortezza et al. 2022*b*, 2022*a*; Isaksson et al. 2025; Jahan et al. 2025). Here

we examine and compare multiple biotic selective pressures hypothesized to be relevant to the evolution of AM, namely both predation of and predation by an aggregative microbe.

Many different types of organisms perform AM, suggesting that it has relevant adaptive benefits (La Fortezza et al. 2022*b*). The best-studied AM species are the amoeba *Dictyostelium discoideum* and the bacterium *Myxococcus xanthus,* the latter being the focus of this study. AM represents a way that organisms can overcome the biophysical limitations of single cells to increase their biological complexity. AM involves complex signaling repertoires that enable cells to encounter one another and regulate their coordinated behaviors, suggesting multi-step evolution and significant benefits to get there (La Fortezza et al. 2022*b*). The lack of a single celled bottleneck, an intrinsic feature of CM, makes AM susceptible to evolutionarily persistent cheating (Grosberg and Strathmann 2007); that it persists further suggests adaptive benefits. Most known forms of AM involve two components: cells assembling into a macro-structure, and differentiation of some cells into a reproductive/stress-resistant sub-population (*e.g.*, spores). This suggests that AM may have originated as a mechanism for responding to biotic threats and/or to survive unfavorable environmental conditions (La Fortezza et al. 2022*b*). The latter hypothesis is supported by the formation of stress-resistant spores within aggregate structures in many AM systems in the lab, whereas the former hypothesis has been less investigated.

Predation has long been studied as a driving force in the evolutionary transition to multicellularity (Stanley 1973; Bonner 1998; Boraas et al. 1998; Claessen et al. 2014; Pentz et al. 2015; Kapsetaki et al. 2016; Herron et al. 2019), and indeed predation has been shown to select for CM in the lab (Herron et al. 2019). Although it has been hypothesized that AM might also provide protection from predation for a variety of aggregative microbes (Kessin et al. 1996; Velicer and Vos 2009; Dahl et al. 2011; Pérez et al. 2011; DePas et al. 2014; Müller et al. 2015), direct study of how predators of AM microbes influence the evolution of their aggregative behaviors and morphologies has been lacking.

We address this gap with a tri-trophic-level evolution experiment involving: (i) the social soil bacterium *M. xanthus* (order Myxococcales, aka ‘myxobacteria’ (Shimkets et al. 2006*a*; Velicer and Vos 2009)) , (ii) *Pristionchus pacificus*, a nematode capable of preying on *M. xanthus* (this study),

(iii) and *Escherichia coli,* a bacterium that serves as prey to both *P. pacificus* and *M. xanthus* (Hong and Sommer 2006; Morgan et al. 2010). All are found in soils and may interact in their natural environment (Hong and Sommer 2006; Morgan et al. 2010). *M. xanthus* aggregates to form spore-filled fruiting bodies (FBs) upon starvation, as well as upon interacting with some other bacterial species (Kroos et al. 2025). *M. xanthus* is well known as a predator, swarming through soil in coordinated groups and preying on a wide range of other microbes, including gram-negative and gram-positive bacteria and fungi (Bull et al. 2002; Morgan et al. 2010; Mendes-Soares and Velicer 2013; Livingstone et al. 2017). *M. xanthus* presumably uses FB formation combined with sporulation for the purpose of better surviving low-nutrient conditions (Kroos 2017). However, it may also use FB formation to better survive predators in the environment. Selection imposed by such predators may have thus contributed to the origin and stunning diversification of fruiting-body morphologies observed among the myxobacteria (Shimkets et al. 2006*b*; Velicer and Vos 2009; La Fortezza et al. 2022*b*; Kroos et al. 2025), as well as among aggregative systems more broadly such as the dictyostelids (Bonner 2009).

Because *M. xanthus* and many other aggregative microbes (*e.g.*, *D. discoideum*) are mesopredators (*i.e.*, predators of other microbes as well as potential prey for higher-order predators), they are ideal for studying multi-step trophic webs in ecological and evolutionary experiments. *M. xanthus* predation on other bacteria has featured in multiple evolution experiments (MyxoEEs, see myxoee.org (Velicer et al. 2024)). In MyxoEE-4, for example, *M. xanthus* adapted its foraging ability in response to prey abundance (Hillesland et al. 2009). In MyxoEE-6, it both adaptively evolved as a predator and drove evolution of prey responses, including changes in virulence traits (Nair et al. 2019; Nair and Velicer 2021). In MyxoEE-3, prey presence and identity were found to indirectly shape the evolution of *M. xanthus* fruiting body phenotypes (La Fortezza et al. 2022*a*).

How mesopredators respond evolutionarily to higher-order predators and how such responses shape the evolution and ecology of food webs are longstanding questions that have nonetheless received relatively little direct experimental attention (Brodie and Brodie 1999; Abrams 2000; Urban 2013). Here we present an evolution experiment in which a bacterial predator – *M.*

106 *xanthus* – functions as a mesopredator in a multi-step food web. This experiment was conducted to
107 test effects of *M. xanthus* both i) carrying out and ii) being subject to predation on the evolution of
108 *M. xanthus* features, including behavioral traits during interactions with both prey and apex
109 predators. In this first evolution experiment with a bacterial mesopredator, we allowed only *M.*
110 *xanthus* to evolve in order to simplify analysis of evolutionary causation. This initial study emerging
111 from the evolution experiment focuses on phenotypic evolution of *M. xanthus* traits related to
112 aggregative development.

113 Here we investigated whether the prey or the apex predator was the primary driver of AM
114 phenotypic evolution, including the effect of each alone and in combination. Replicate populations of
115 *M. xanthus* evolved in each of four selective regimes that differed only in the presence or absence
116 of two non-evolving biotic partners – *E. coli* as the basal prey and *P. pristionchus* as the apex
117 predator (Figure 1A). The ancestral *M. xanthus* strain underwent aggregative development after
118 limited growth on the experimental medium, due to amino acid restriction. There was therefore the
119 potential for the prey and/or apex predator to impose direct selection on features of *M. xanthus*
120 development. CFcc limits *M. xanthus* growth through amino acid restriction (Bretscher and Kaiser
121 1978) without similarly limiting *E. coli* growth (Kreth et al. 2013) (Figure 1A). Importantly, after
122 depleting growth substrate from the nutrient agar, *M. xanthus* underwent aggregative development
123 within each weekly evolution cycle in the absence of any biotic partners, creating the potential for
124 addition of the basal prey and/or apex predator to impose direct selection on developmental
125 features. To address the effect of the prey and the apex predator on mesopredator evolution, we
126 quantitatively compared several developmental traits – including fruiting body number, fruiting body
127 density, and spore production – between evolved populations their ancestors, and among evolution
128 treatments.

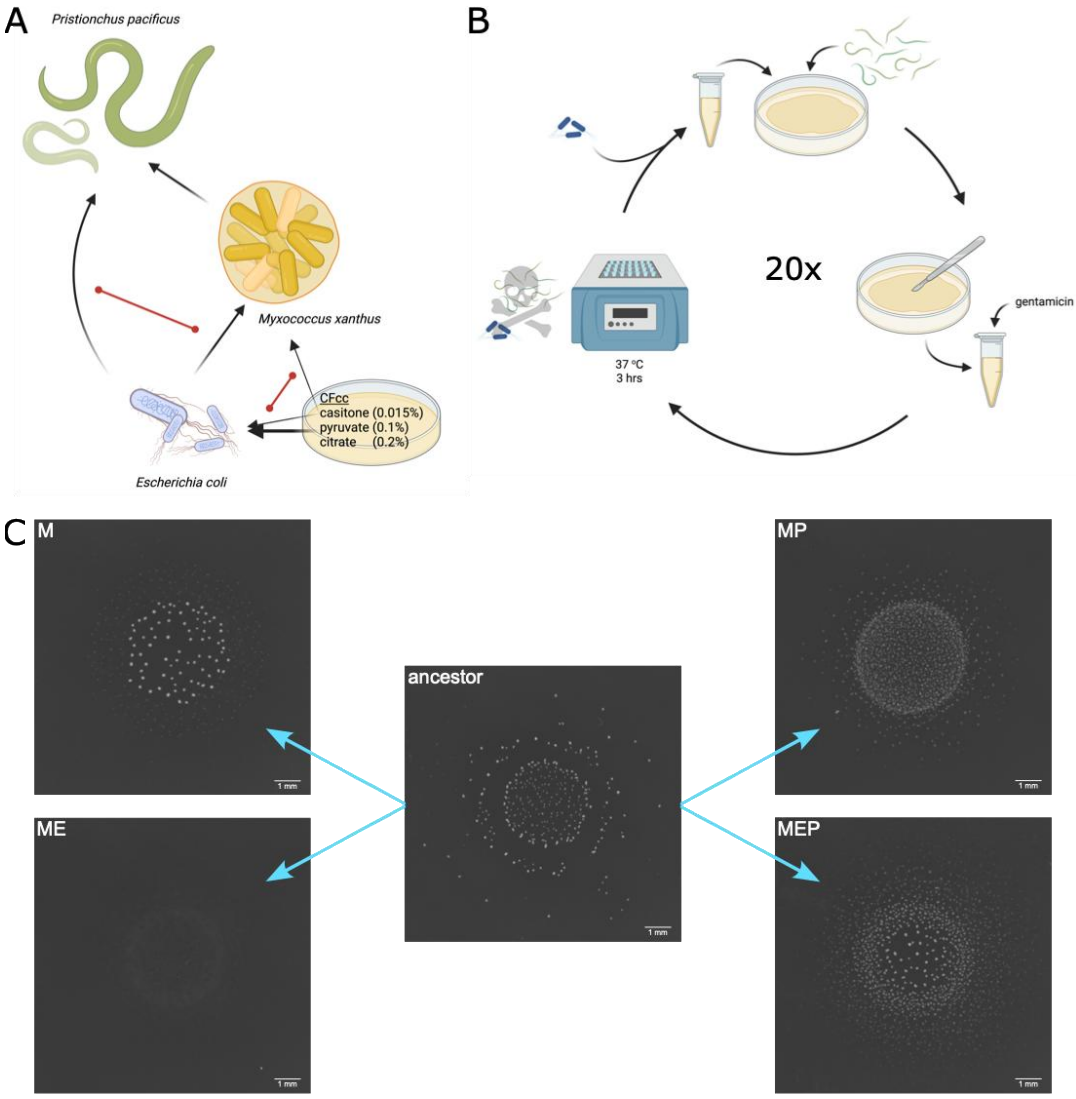

Figure 1. Experimental food web and evolution protocol. (A) We assembled a tri-trophic food web with *P. pacificus* as the apex predator, *M. xanthus* as the mesopredator, and *E. coli* as the basal prey.. Black arrows indicate energy flow (*e.g.,* via predation). Red double-headed lines indicate competition for resources. (B) Schematic showing the regime by which *M. xanthus* was transferred from cycle to cycle during the evolution experiment. (C) Images representing developmental diversification among evolved lineages. Images have been cropped, set to greyscale, and inverted for clarity. All images from the same ancestor. Panels A and B were created with BioRender.com.

142 **Methods**

143

144 *Organisms*. Our focal organism was *M. xanthus*, whose social traits and evolution in biotic context is
145 of particular interest to us. Here we used the well-characterized *M. xanthus* lab strain GJV1 (Velicer
146 et al. 2006) (strain 'S' in (Velicer et al. 1998)), as well as GJV2, a spontaneous mutant of GJV1
147 which is resistant to rifampicin (strain 'R' in (Velicer et al. 1998)). GJV2 differs from GJV1 by a
148 single mutation in *rpoB*, the β-subunit of RNA polymerase (Zee et al. 2014). We used this antibiotic-
149 resistant variant of GJV1 to initiate half of our populations to allow us to directly compete evolved
150 populations against the reciprocally marked ancestor and distinguish them through selective plating
151 during subsequent assays. We chose GJV2 because in previous studies it did not exhibit significant
152 defects in either group swarming (Velicer et al. 2002) or development (Manhes and Velicer 2011),
153 and we therefore did not expect substantial differences in trait evolution during trophic interactions.
154 Previous work indicates that *C. elegans* is not an effective predator of *M. xanthus* (Mayrhofer
155 et al. 2021), so we used *Pristionchus pacificus* PS312 (Hong and Sommer 2006) as the apex
156 predator. We observed that under laboratory conditions, *P. pacificus* is able to grow and reproduce
157 when *M. xanthus* is given as the only food source (Figure 2). For the basal prey, we used *E. coli*
158 OP50, which is a commonly used laboratory prey of nematodes (Brenner 1974).

159

160 *Bacterial growth conditions*. We maintained 20%-glycerol freezer stocks of bacterial strains at -80
161 °C. We inoculated *M. xanthus* strains onto CTT 1.5% agar plates (Bretscher and Kaiser 1978) and
162 incubated at 32 °C and 90% rH for 4 days, then transferred a portion of the colony into CTT liquid
163 and incubated overnight at 32 °C with shaking at 300 rpm until the cultures reached mid-log phase
164 (OD_{595} 0.2 - 0.8). We inoculated *E. coli* strains directly into lysogeny broth (LB) and incubated
165 overnight at 32 °C with shaking at 300 rpm.

166

167 *Culturing nematodes*. We maintained freezer stocks of *P. pacificus* at -80 °C. We prepared freezer
168 stocks according to Pires da Silva (Pires da Silva 2013). We collected worms from recently starved
169 plates with Freezing Solution (100 µl/ml DMSO and 0.1 g/ml Dextran in water), aliquoted 1-ml

170 volumes into freezer vials, and allowed them to freeze slowly in a Nalgene® Cryo 1°C Freezing
171 Container containing isopropanol. To revive worms, we thawed an entire freezer vial, transferred
172 the contents to a Falcon tube with a Pasteur pipette, added 10 ml of Thawing Solution (300 mg/L L-
173 glutamine in M9 buffer [5 g/L NaCl, 6 g/L Na_2HPO_4, 3 g/L KH_2PO_4, and 1 mM $MgSO_4$ in water]),
174 centrifuged for 1 min at 150 x *g*, and removed the supernatant. We then transferred the thawed
175 worms to the edges of *E. coli* OP50 lawns on 2% agar NGM (Stiernagle 2006) or HGM (Kauffman
176 et al. 2011) plates. We incubated the plates at 25 C and 50% rH.
177
178 *Bleaching nematodes*. We bleached *P. pacificus* as in Mayrhofer *et al.* (Mayrhofer et al. 2021) to
179 create synchronized cultures to use in experiments. We washed nematodes from HGM plates using
180 M9 buffer and collected them in a 15-ml Falcon tube. We centrifuged them for 1 min at 173 x *g* and
181 removed all supernatant except 500 µl, to remove as much *E. coli* OP50 as possible. We added 1
182 ml of fresh M9 so that the total volume was 1.5 ml, then added 3 ml of bleaching solution (6 ml H_2O,
183 6 ml NaOCl 5%, 2 ml 5M NaOH) and bleached with periodic vortexing until most of the adult bodies
184 had dissolved, up to 7 minutes. We removed the bleach from the released eggs by centrifuging for 1
185 min at 173 x *g*, removing all but 500 µl of supernatant, and adding 4.5 ml sterile water. We washed
186 the eggs four times, and after the fourth wash removed all but 500 µl of supernatant and added 3.5
187 ml M9. We used a Pasteur pipette to transfer the egg suspension to a 6-cm petri dish and added 1
188 µg/ml gentamicin to prevent any possible *E. coli* contamination. We allowed the eggs to hatch
189 overnight. We removed dauer pheromone, which is released when food availability is low and
190 inhibits nematode growth and development, and counted the number of hatched J2 larvae by
191 centrifuging the worms in a 15-ml Falcon tube for 1 min at 173 x *g*, removing as much supernatant
192 as possible, adding M9 up to 1 ml, and counting in triplicate 1-µl aliquots plated on sterile CFcc
193 1.5% agar plates (Mayrhofer et al. 2021).
194
195 *Nematode predation tests*. To quantify population reduction of *M. xanthus* by *P. pacificus*, we
196 prepared 6-cm petri dishes filled with 11 ml of CFcc 1.5% agar, inoculating ~2 x 10^6 CFUs GJV1 as
197 the food source and spreading with glass beads. We added ~200 J2 *P. pacificus* larvae in 100 µl

198 M9 or 100 µl of sterile M9 as a predator-free control and incubated at 25 °C and 50% rH. After 1
199 day, 4 days, and 7 days we destructively harvested all biological material from agar surfaces with a
200 sterile scalpel and transferred to the center of a 9-cm CTT 0.5% agar plate. We measured the
201 diameter of the swarm size of the surviving *M. xanthus* population after 4 days and used a standard
202 curve relating swarm size to inoculum size to estimate *M. xanthus* population sizes (approach
203 adapted from (Rendueles and Velicer 2017), Fig. S5). We calculated the area under the curve and
204 used a general linear model to test for differences with and without worms.
205 To quantify reproduction of *P. pacificus* using only *M. xanthus* as a food source, we
206 inoculated 3 x 10^9 cells of GJV1 or 300 µl sterile TPM buffer in the center of TPM 1.5% agar plates,
207 picked 3 J4 *P. pacificus* larvae onto each plate, and incubated at 25 °C and 50% rH for 3 days. To
208 count the worms, we washed the plates with 1 ml of TPM buffer, counted the number of worms
209 present in 3 aliquots of 30 ul, and counted the number of worms remaining on each plate. For buffer
210 plates, we only counted the worms present on the plates. We used a Mann-Whitney U-test to
211 compare the two treatments.
212
213 *Evolution experiment*. We isolated 6 clones each from GJV1 and GJV2 and named them 11-16 and
214 21-26, respectively (hereafter referred to collectively as 'A' for 'ancestor'). We used each of these
215 clones to found four populations, one in each of the evolution treatments. The evolution treatments
216 were *M. xanthus* evolving in monoculture (M), *M. xanthus* evolving in co-culture with non-evolving
217 *E. coli* (ME), *M. xanthus* evolving in co-culture with non-evolving *P. pacificus* (MP), and *M. xanthus*
218 evolving in co-culture with non-evolving *E. coli* and non-evolving *P. pacificus* (MEP). We performed
219 the experiment on CFcc 1.5% agar plates (Hagen et al. 1978; Mayrhofer et al. 2021), which contain
220 0.015% casitone as the only source of amino acids, as well as 0.1% pyruvate and 0.2% citrate. *M.*
221 *xanthus* must exogenously acquire several amino acids (Bretscher and Kaiser 1978) and was
222 therefore more limited in monoculture growth on experimental CFcc plates than *E. coli* OP50, a
223 leaky uracil auxotroph (Brenner 1974). Both citrate and pyruvate stimulate *M. xanthus* growth in the
224 presence of exogenously provided amino acids, with pyruvate stimulating greater growth (Bretscher

225 and Kaiser 1978); once the casitone was depleted, *M. xanthus* would be unable to continue growing
226 on the provided carbon sources.

227 To initiate the experiment, we added ~2 x 10^6 CFUs of each founding clone, pre-mixed with
228 ~10^9 CFUs of *E. coli* for ME and MEP treatments, to 6-cm petri dishes filled with 11 ml of CFcc
229 1.5% agar. We spread the bacterial inoculum with glass beads until dry, removed the glass beads,
230 and added ~200 J2 *P. pacificus* larvae in 100 µl M9 (for MP and MEP treatments) or 100 µl of
231 sterile M9 (for M and ME treatments). We sealed the plates with parafilm and incubated for 7 days
232 at 25 °C and 50% rH.

233 To passage *M. xanthus* at the end of each cycle, we harvested the biological material from
234 the surface of each evolution plate with a sterile scalpel and washed it into an Eppendorf tube with 1
235 ml of CFcc liquid with 1 µg/ml gentamicin to kill the *E. coli*. We incubated the tubes in a dry bath at
236 37 °C for 3 hrs (to kill the worms). We then transferred 1% of the volume of each culture to a new
237 evolution plate (pre-mixed with either *E. coli* or buffer). We continued for a total of 20 cycles (Figure
238 1B). Six populations were lost due to contamination, leaving 42 evolved populations at the end of
239 cycle 20.

240 At the end of even-numbered cycles, we transferred the remaining volume from the finished
241 cycle to CTT liquid and allowed *M. xanthus* to grow up overnight in shaken culture at 32 °C and 300
242 rpm, then prepared 20%-glycerol freezer stocks. All following work was performed on population
243 samples from terminal freezer stocks.

244

245 *Fruiting body morphology assay*. We observed and quantified the fruiting body phenotypes of
246 terminal evolved populations and their ancestral clones as in La Fortezza and Velicer (La Fortezza
247 and Velicer 2021). We grew liquid cultures of cycle-20 evolved populations as described above. We
248 diluted them and allowed them to shake overnight again in order to ensure that the resulting
249 cultures would be as free from clumps as possible. We centrifuged them at 12,000 rpm for 5 min
250 and resuspended to 5 x 10^9 CFUs/ml in TPM buffer. We poured 5 ml of CFcc 1.5% agar into 6-cm
251 petri dishes and allowed to dry. We plated 10 µl of each population and allowed the spots to dry for
252 1 hr, then incubated at 25 °C and 50% rH for 7 days. Due to limitations on sample handling time

253 during assay plate preparation, we processed in 5 blocks per replicate of 11 populations at a time.
254 Each block also included GJV1 and GJV2 as internal controls. This resulted in 13 samples per
255 block, and 20 total blocks.
256 After 7 days, we imaged the samples (Figure 1C) using an Olympus SZX16 microscope and
257 Olympus DP80 camera together with cellSens software version 1.15 (Olympus, Tokyo, Japan),
258 according to La Fortezza and Velicer (La Fortezza and Velicer 2021). Microscope, camera, and
259 software settings were the same for all samples across all blocks and replicates. Images are
260 available via the BioImage Archive (DOI). To check for correlations between fruiting body
261 morphology and spore production, we then harvested all biological material using flame-sterilized
262 scalpels, sonicated to disperse aggregates, and quantified spore production by counting the number
263 of spores (identified by spherical shape and high refractivity) in a given area of a Neubauer
264 improved hemocytometer.
265
266 *Image processing*. We analyzed the images using Fiji version 1.53q (Schindelin et al. 2012). We
267 converted each image to 8-bit, removed dust particles and other non-bacterial parts of the image,
268 and set the black-white threshold to capture all aggregates. We saved this information as an overlay
269 which we applied to the original image to collect data on the aggregates. We quantified fruiting body
270 morphology with four traits previously used for this purpose (Rivera-Yoshida et al. 2019; La
271 Fortezza and Velicer 2021): number of aggregates, size of each aggregate (pixels^2), average grey
272 value of each aggregate (density in La Fortezza and Velicer 2021), standard deviation of grey
273 values within each aggregate (density heterogeneity in La Fortezza and Velicer 2021), and x and y
274 coordinates of each aggregate. The 1 mm scale bar (Figure 1C) corresponds to 293 pixels; 1 pixel =
275 ~3.5 nm. Fruiting body density is inversely related to transparency and positively correlated with
276 fruiting body maturity and spore content; here we use an arbitrary scale between 0 and 200. Density
277 heterogeneity quantifies within-aggregate texture variation. A full description of these traits is given
278 in (Rivera-Yoshida et al. 2019; La Fortezza and Velicer 2021).
279

280 *Fruiting body trait analysis.* We analyzed fruiting body morphological traits and spore production in
281 R version 4.1.3 (R Core Team 2024) and RStudio version 2022.02.1+461 (RStudio Team 2020).
282 We analyzed overall fruiting body morphology according to the method established by La Fortezza
283 *et al*. (La Fortezza and Velicer 2021), by principal components analysis followed by PERMANOVA
284 using the *adonis2* function in the "vegan" package (Oksanen et al. 2020) to check for effects of
285 evolution environment. All trait data (fruiting body number, area, mean grey value, and density
286 heterogeneity) were standardized (centered and scaled to unit variance) prior to PCA using the R
287 command *prcomp()*, and we tested for homogeneity of multivariate dispersions using the
288 *vegan::betadisper()* function. We further analyzed fruiting body traits individually using ANOVA to
289 test for effects of evolution environment and of ancestral genotype (GJV1 or GJV2, from which we
290 picked the 12 founding clones used to start the evolution experiment) followed by Tukey HSD tests
291 for differences from the founding clones and among evolution treatments. We analyzed spore
292 production data the same way, ANOVA for differences based on evolution environment and GJV1
293 versus GJV2 ancestry followed by Tukey HSD tests. Data occasionally violate normality or
294 homoscedasticity. Non-parametric models (Kruskal-Wallis tests with Conover-Iman post-hoc tests)
295 produce similar results to parametric ones and are less conservative; here we report results from
296 parametric models to allow comparison of treatment means. The data files and full statistical
297 analysis are available via Zenodo (DOI). There were different numbers of surviving populations per
298 evolution treatment and *rpoB* ancestry. For GJV1 lineages, M = 5, ME = 6, MP = 5, MEP = 4. For
299 GJV2 lineages, M = 5, ME = 6, MP = 5, MEP = 6. We replicated the post-evolution development
300 assay 4 times, resulting in 4 replicates per lineage, and therefore ≥16 assay values per evolution
301 treatment. Figures were generated using the "ggplot2" package (Wickham 2016).
302
303 *Morphological integration analysis*. We tested morphological integration of fruiting body traits by
304 analyzing eigenvector variance of the trait morphospace of the four developmental traits following
305 previously established methods (Pavlicev et al. 2009; Machado et al. 2019; La Fortezza et al.
306 2022*a*). Traits were standardized prior to computing covariance matrices. For this analysis, we
307 included spore production as a trait. We calculated covariance matrices of the five traits for each

evolution treatment individually and eigenvector variances (Var(λ)) using *CalcEigenVar()* in the "evolqg" package (Melo et al. 2016). Figures were generated using the "ggplot2" package (Wickham 2016).

Time-lapse assay. We performed a time-lapse fruiting body morphology assay on GJV1-descended lineages from cycle 20 developing on CFcc media, initiated as described above. We imaged the samples using the Olympus SZX16 microscope and Olympus DP80 camera with cellSense software version 4.3 (Olympus, Tokyo, Japan) every 24 hours for seven days. The settings were kept identical throughout all replicates (exposure time = 1.67ms, lens = Olympus 0.5x PF, zoom = 1.25, ISO = 200, illumination = BF built-in system). We performed four independent replicate observations of each lineage.

We processed and analyzed the images with Fiji version 1.54p, using the same technique as the described above with the addition of excluding all particles under 30 pixel^2 before overlaying onto the original image. For samples without fruiting bodies, we set the number of aggregates to one, average grey value to 50, the mean standard grey value to 0.18, and the area of the aggregate to 30 pixel^2. This corresponded to one very small, pale and homogeneous fruiting body on the entire plate. We generated an artificial starting point (t = 0 hour) using the same values to improve readability of the graphs. We performed a principal component analysis as above using R version 4.1.3 (R Core Team 2024) and RStudio version 2022.02.1+461 (RStudio Team 2020), and generated figures using the "ggplot2" package (Wickham 2016).

Results

P. pacificus successfully preys on M. xanthus. To confirm whether *P. pacificus* acts as an apex predator in this system, we tested its ability to reproduce and consume *M. xanthus* as a sole food source. *P. pacificus* significantly reduces *M. xanthus* population size (Figure 2A; one-way ANOVA for area under the curve, $F_{1,20} = 6.94$, $p = 0.039$, difference = 86.5% reduction at final time point),

335 and is able to complete development to adulthood and reproduce successfully (Figure 2B; Mann-
336 Whitney U-test, n = 4, W = 0, p = 0.02, difference = 41 worms).
337

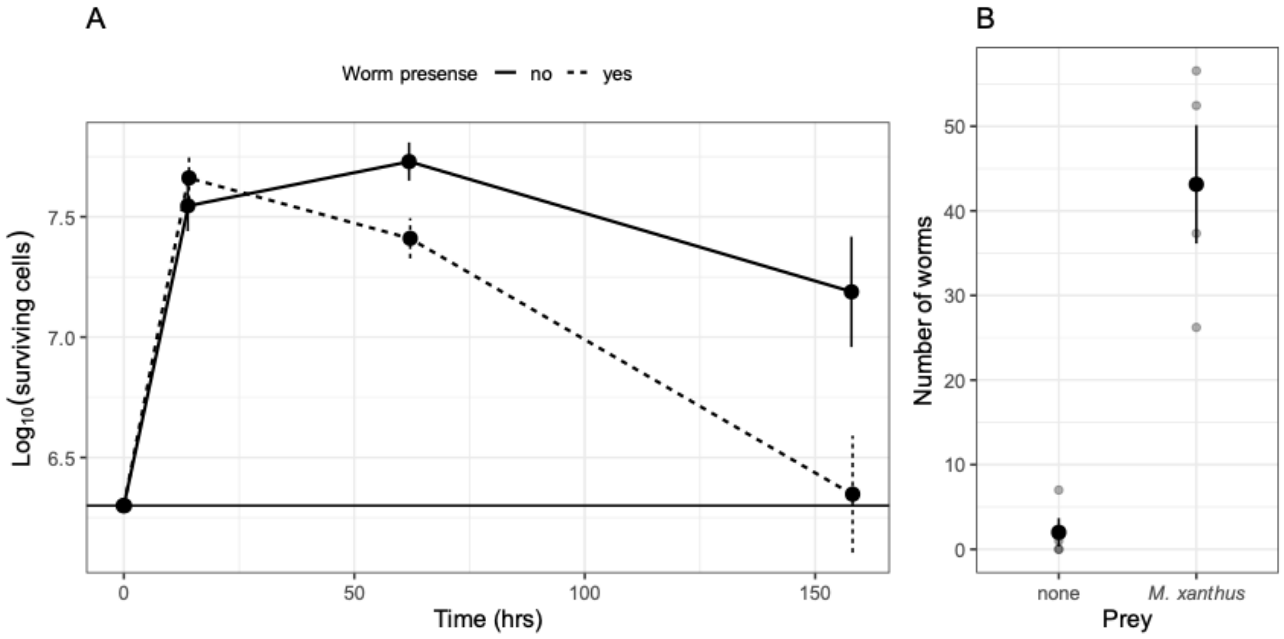

338

339 **Figure 2. *Pristionchus pacificus* predation of *Myxococcus xanthus*.** We cultured *P. pacificus* on *M. xan-*
340 *thus* as the sole food source. (A) Population dynamics of *M. xanthus* under predation by *P. pacificus*. Dots are
341 averages of four biological replicates. The horizontal line shows the initial population size of *M. xanthus*. (B) *P.*
342 *pacificus* reproduction on *M. xanthus*. Initial populations were founded with three J4 larvae. Large black dots
343 are averages of four biological replicates. Error bars represent standard error. Small grey dots show individual
344 replicates. *P. pacificus* population sizes after 72 hours are shown.
345

346 *rpoB-mutant lineages show far less trait evolution in communities than wild-type lineages.* We
347 anticipated change in phenotypes related to multicellular development over evolutionary time in all
348 treatments, as well as phenotypic diversification as a function of treatments, as such traits are
349 relevant to nutrient levels, prey presence and type (La Fortezza et al. 2022*a*), and we hypothesized
350 also to anti-predator defense (La Fortezza et al. 2022*b*). We therefore examined four traits related
351 to fruiting body morphology in the evolved populations and their ancestral clones: the number of
352 fruiting bodies produced by each population, their average size, their average density (darkness of

353 color, with darker aggregates generally being more mature and containing more spores), and the
354 average heterogeneity of density.

355 In the evolution experiment we included six lineages per treatment descending from GJV1
356 (wild-type) and six descending from GJV2 (spontaneous rifampicin-resistant *rpoB* mutant), to allow
357 the possibility of competing oppositely-marked strains head-to-head during follow-up assays. We
358 chose this design because these strains have been used this way before (Velicer et al. 2002;
359 Manhes and Velicer 2011). However, observations during the evolution experiment indicated that
360 lineages founded from the two strains showed different patterns of evolution. We therefore
361 performed an initial analysis of the principal components of variation among the four morphology
362 traits based on ancestral genotype (GJV1 or GJV2), including the 12 ancestral clones and all
363 surviving populations from the four evolution treatments from the final timepoint (N = 26 for GJV1, N
364 = 28 for GJV2). In the resulting PCA plot (Figure 3A), descendants of GJV2 cluster more closely
365 together, indicating less evolutionary divergence from the ancestral clones and among evolution
366 treatments than for lineages descending from GJV1. Although previous studies found no significant
367 differences compared to wild-type swarming and development phenotypes (Velicer et al. 2002;
368 Manhes and Velicer 2011), the *rpoB* mutation likely affected GJV2 descendants' ability to evolve in
369 response to evolutionary conditions. We therefore analyzed principal components of trait variation
370 for GJV1 and GJV2 descendants separately.

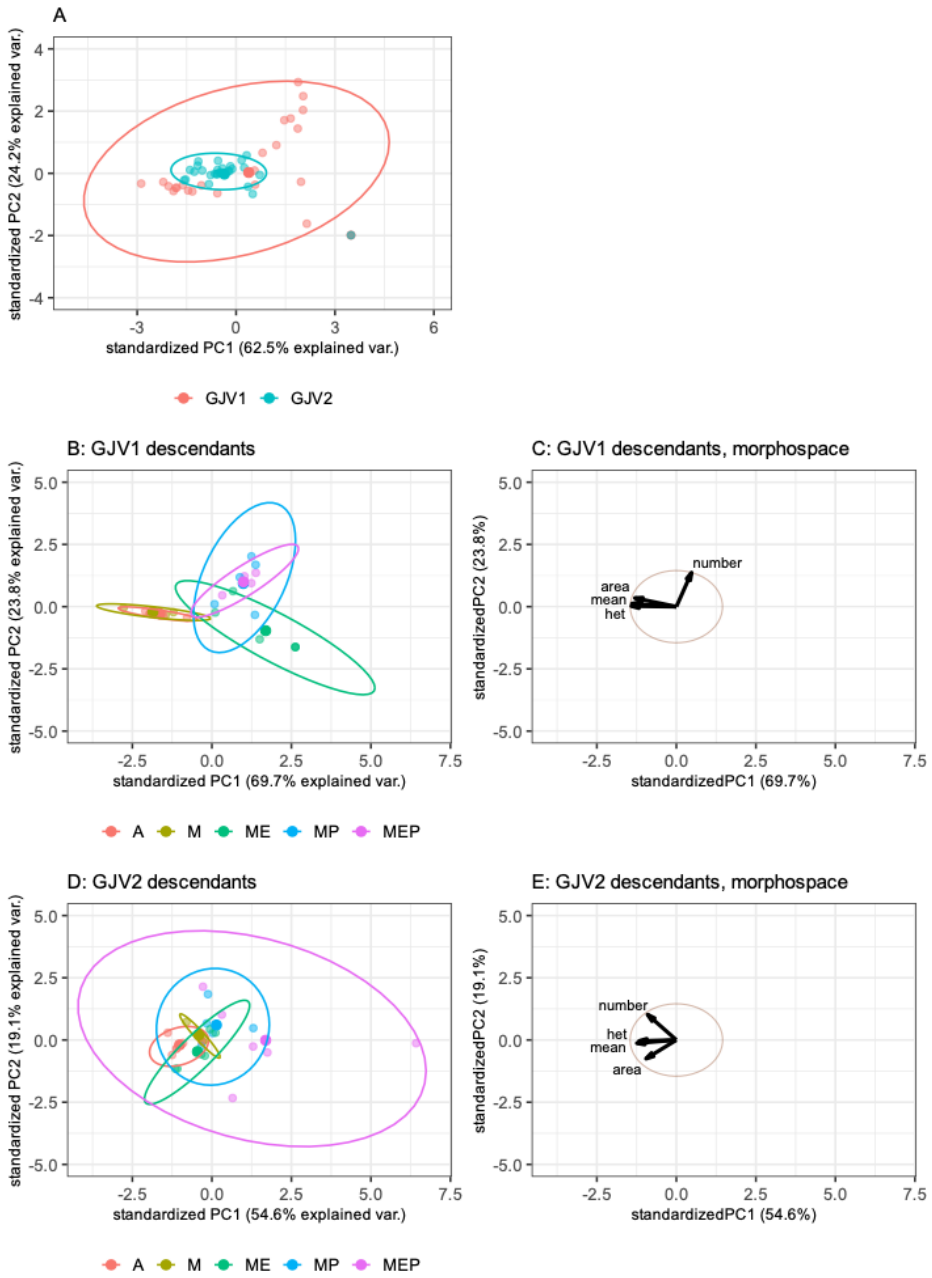

Figure 3. Evolutionary variation depends on ancestral genotype. We analyzed morphologies of fruiting bodies produced by *M. xanthus* populations that had evolved alone (M), in the presence of *E. coli* (ME), in the presence of *P. pacificus* (MP), or in the presence of both (MEP), as well as the clones used to found the evolved populations (A). Six of the founding clones come from GJV1 and six come from GJV2. We measured the principal components of variation across fruiting body traits. Here we show overall variation in fruiting body morphology as a function of the ultimate ancestor of the clones or evolved populations in the form of a principal components analysis of the four traits. Panel A shows the phenotypic variation within descendants of GJV1 versus descendants of GJV2. Panels B & D show trait variation based on evolution environment. Small

381 dots represent averages across four replicates for each surviving lineage, large dots represent the centroid of
382 each group (the average of PC1 and PC2 across all replicate lineages) and ellipses represent the 95%
383 confidence region. Percentages listed in the x- and y-axis titles are the percent of variation within the dataset
384 which is explained by that principal component. Panels C & E visualize the morphospaces, which consider
385 how the four traits correlate, and which can be used to interpret the variation seen in panels B & D. Arrows
386 indicate the directional effect of each trait on the morphospace – along that vector, the value of the indicated
387 trait increases. Traits: “het” = fruiting body heterogeneity, “area” = fruiting body size, “mean” = fruiting body
388 darkness, “number” = number of fruiting bodies produced by a defined population of cells.
389
390 GJV1 lineages show significant variation among the five groups (evolved populations and
391 ancestral clones; Figure 3B; PERMANOVA for effect of treatment, $F_{4,21} = 16.99$, $p < 0.001$). GJV2
392 lineages also vary (Figure 3D; PERMANOVA for effect of treatment, $F_{4,23} = 3.25$, $p = 0.002$),
393 although trait differences are smaller in magnitude than for wild-type lineages (Figure 4). Further,
394 we see different patterns of evolved integration, or pleiotropic correlation, across fruiting body
395 morphology traits (Figure S1).
396
397 *The apex predator drives evolution of fruiting body number in GJV1 descendants*. Two striking
398 results emerged from the PCA of the fruiting body morphologies of GJV1 descendants. First, we
399 see clear divergence of all three treatments with multi-species communities (ME, MP and MEP);
400 Figure 3B, green, blue and purple ellipses, respectively) from the founding clones (A) and the M
401 populations (Figure 3B red and yellow ellipses, respectively). Second, we also observe clear
402 divergence of the two multi-species treatments that included nematodes (MP and MEP) from the
403 one that did not (ME).
404 Quantifying individual traits (Figure 4), we see that MP and MEP populations produce more
405 fruiting bodies that are also smaller, less dense, and less heterogenous, while the founding clones
406 and the M populations produce fewer fruiting bodies that are relatively larger, denser, and more
407 heterogenous (Figure 1C, representative images). In greater detail, populations which evolved in
408 the presence of *P. pacificus* (MP and MEP) show significantly higher numbers of fruiting bodies

409 than the founding clones or the M or ME lineages (Figure 4; Tukey HSD tests, p's < 0.002,
410 differences > 855). This effect is independent of the presence of *E. coli* (Tukey HSD test, $p_{MP:MEP}$ =
411 0.99, difference = 73). Fruiting body number of M and ME treatments did not diverge from the
412 ancestral phenotype (Figure 4; Tukey HSD tests, p's > 0.98). GJV2 descendants do not show a
413 similar trend of phenotypic change (Figure 4; one-way ANOVA for effect of treatment, $F_{4,23}$ = 0.76, p
414 = 0.56). Together, this indicates that increasing the number of fruiting bodies produced by a
415 population of a given size is an evolutionary response specific to the presence of worms, but that
416 the *rpoB* mutation in the GJV2 lineages inhibits this response.

417 We hypothesized that MP and MEP lineages produced more, smaller fruiting bodies
418 because they entered development earlier than other lineages, possibly as a defensive adaptation
419 to the presence of *P. pacificus*. To test this hypothesis, we conducted a time lapse experiment,
420 allowing all lineages to develop as in the previous assay and imaging them at 24-hour intervals.
421 While MP and MEP lineages show differing developmental trajectories compared to the other
422 treatments, as expected from the above results, they do not show evidence of earlier initiation of
423 development (i.e., increased distance of day 1 from t=0 than other treatments; Figure 5A). The
424 number of fruiting bodies observed in MP and MEP lineages generally increases between days 1
425 and 3 after initiation of the experiment, whereas the fruiting bodies of the ancestral clones (A) seem
426 to have developed within the first 24 hours (Figure 5B). Overall, these results indicate that the
427 increased number and smaller size of MP and MEP fruiting bodies is not a result of the population
428 initiating development earlier, before cells have had a chance to aggregate in greater numbers.
429

430 *Evolution in multi-species communities reduces individual-fruiting-body trait values and promotes*
431 *morphological trait integration*. The PCAs in Figure 3B and 3D suggest little overall divergence
432 between phenotypes of populations that evolved in monoculture and phenotypes of the ancestral
433 clones (*i.e.,* the red and yellow ellipses are largely overlapping, indicating that they represent
434 groups with similar trait values). In line with this, the individual trait analyses (Figure 4) show that
435 the M populations evolved to differ from the ancestral phenotype only in fruiting body size, and not
436 at any of the other three traits. The average fruiting body size of the M populations increased

437 significantly relative to the average values for the other evolution treatments (Tukey HSD tests,
438 $p_{M:ME}$ < 0.0001 difference = 755 pixels^2 (2.58 mm^2), $p_{M:MP}$ = 0.0009 difference = 550 pixels^2 (1.88
439 mm^2), $p_{M:MEP}$ = 0.009 difference = 460 pixels^2 (1.57 mm^2)), although the difference relative to the
440 ancestor was not significant (p = 0.06, difference = 319 pixels^2 (1.09 mm^2)). The average size of ME
441 fruiting bodies decreased relative to the ancestor (Tukey HSD test, p < 0.004 difference = 436
442 pixels^2 (1.49 mm^2)), although this is most likely due these populations no longer producing mature
443 fruiting bodies.

444 Contrary to the increase in fruiting body number seen in MP and MEP populations
445 descending from GJV1, there are broad decreases in other trait values across all three treatments
446 with multi-species communities (Figure 4). GJV1 descendants that evolved under ME, MP, or MEP
447 conditions all form significantly less dense and less heterogeneous fruiting bodies than both the
448 ancestor (Tukey HSD tests, p's < 0.0002, grey value differences >30, heterogeneity differences
449 >12) and the M-evolved populations (Tukey HSD tests, p's < 0.003, grey value differences >24,
450 heterogeneity differences >11). In addition, ME fruiting bodies are less dense than MEP (Tukey
451 HSD test, p = 0.004, difference = 23). Both metrics refer to pigmentation of the fruiting bodies,
452 measured as grey value of the pixels arbitrarily scaled from 0 to 200. Higher density correlates with
453 more mature fruiting bodies containing greater numbers of spores; higher density heterogeneity
454 indicates greater texture variation on the outer surface of the fruiting body. That these traits did not
455 also decrease among the M populations points to evolutionary responses specific to the presence
456 of biotic partners rather than a generic response to abiotic conditions.

457 Evolution in ME, MP, and MEP conditions increased covariance of fruiting body traits. To
458 investigate general trends in morphological trait integration related to evolution environment, we
459 calculated eigenvector variances (Var(λ)) for the four traits plus spore production for the four
460 environments and the ancestral clones. Var(λ) of 0 indicates no observed correlation among traits,
461 while Var(λ) of 1 indicates that most variance among traits is explained by the first principal
462 component, suggesting stronger covariation (Pavlicev et al. 2009). The ancestral state has
463 eigenvector variance of 0.5, showing partial correlation among the morphological traits. This

464 increases for M, and increases to nearly 1 for ME, MP, and MEP (Figure S1). This suggests that
465 evolution in multi-species communities caused *M. xanthus* developmental traits to evolve in a more
466 integrated manner than did evolution in single-species populations.

467 Populations descending from GJV2 also showed some evolution at traits other than fruiting
468 body number, but changes were smaller overall than for GJV1-descendants (as expected from the
469 PCA in Figure 3A). All evolution treatments except for M form less-dense fruiting bodies than the
470 ancestor (Tukey HSD tests, p's < 0.05, differences >18). MEP populations show divergence in
471 density heterogeneity from M- and ME-evolved populations (Tukey HSD tests for differences among
472 evolution environments, p's < 0.02, differences >7).

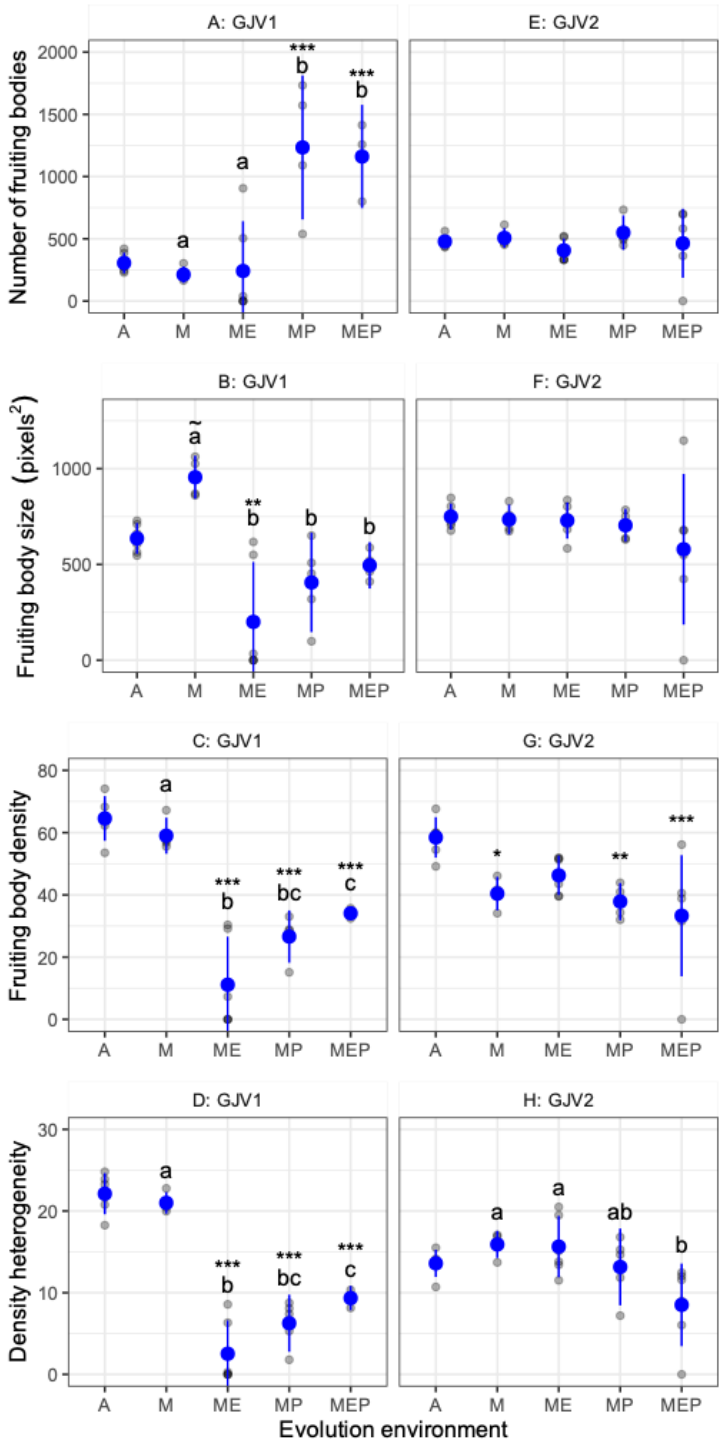

Figure 4. Fruiting body traits show evolutionary responses to community structure. Each measured trait of fruiting body morphology – number, size, density, and density heterogeneity – is plotted individually. We observe differences from the ancestral phenotype, represented by the founding clones (A on the x-axes) and differences among evolution treatments. Small grey dots show the mean of each evolution lineage across 3-4 biological replicates, large blue dots represent the mean across 4-6 replicate lineages, and blue bars

480 show 95% confidence intervals of cross-lineage means. Asterisks indicate difference from the ancestors: ~ =
481 $p < 0.06$, * = $p < 0.05$, ** = $p < 0.01$, *** = $p < 0.005$. Letters indicate statistical groups of evolution treatments
482 that do not differ within groups but differ between groups ($p < 0.05$). Vertical panels group clones or
483 populations descending from GJV1 or from GJV2.
484
485 *Interaction between the apex predator and basal prey causes unexpected phenotypic evolution*. If
486 the selective effects of the basal prey and the apex predator on *M. xanthus* phenotypic evolution
487 were additive, we would expect trait values in the MEP treatment, which exposed *M. xanthus* to
488 both, to fall in between those for ME and MP treatments. However, instead we see striking
489 deviations from this expectation for two individual fruiting body traits – density and density
490 heterogeneity (Fig. 4C-D). If one starts with MP as a reference point and then considers that the ME
491 result would predict that the MEP value should be lower than the MP value under the assumption of
492 linearity, we see that inclusion of *E. coli* in the MEP populations has the opposite effect, causing
493 these three trait values to evolve to higher levels than in the MP populations rather than lower. And
494 using ME as the starting reference point, inclusion of *P. pacificus* in the MEP treatment increases
495 the trait values more than predicted from the ME and MP data alone. Thus, the effects of *E. coli*
496 and *P. pacificus* on *M. xanthus* evolution interact in a nonlinear manner.
497

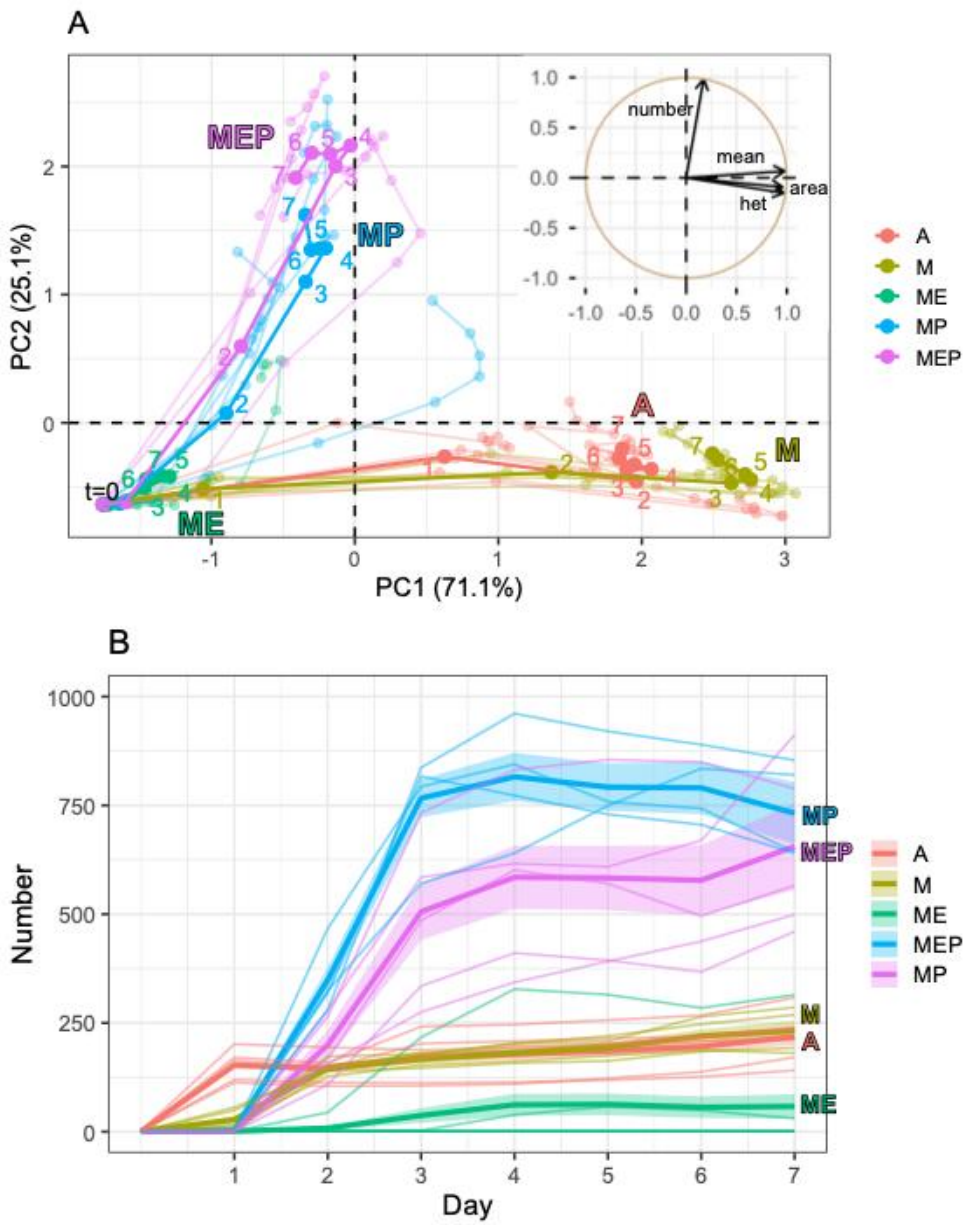

Figure 5. Development over seven days. We imaged development of evolved *M. xanthus* populations over seven days. (A) PCA trajectories of fruiting body morphology. Solid dots and lines show averages per treatment. Transparent dots and lines show individual lineages, averaged over four biological replicates. Numbers indicate the days since the start of the experiment. The trajectory starting point (t=0) was calculated as described in the Methods. Inset shows trait morphospace. Traits: “het” = fruiting body heterogeneity, “area” = fruiting body size, “mean” = fruiting body darkness, “number” = number of fruiting bodies produced by a defined population of cells. (B) The number of fruiting bodies produced over time. Thicker lines show treatment averages, with ribbons indicating standard error. Thinner lines show individual lineages, averaged over four replicate observations.

509 *Nematodes prevent evolutionary reduction of M. xanthus sporulation caused by E. coli alone*. Given
510 the significant changes in fruiting body numbers and several traits of individual fruiting bodies, such
511 as size, we hypothesized that there may be correlated changes in the number of spores produced
512 by those populations and associated treatment-level effects. We paired each measure of fruiting
513 body number and size with the number of spores counted from that plate (Figure S2). Spore
514 production correlates positively with both of these traits (Table S1). For descendants of GJV1, the
515 correlation with fruiting body size differs based on evolution environment (Table S1; two-way
516 ANOVA for effects of area and treatment on spore production, $F_{4,16} = 3.132$, $p = 0.044$), but in every
517 other case the effects are independent.

518 When looking at spore production only (Figure 6) overall across populations descended from
519 both ancestors (GJV1 vs GJV2), most treatments showed no significant change or moderate
520 increases in spore production. Exceptionally, however the ME populations decreased ~90% in
521 spore production on average. The absence of a corresponding decrease in the MEP lines indicates
522 that the presence of *P. pacificus* prevented selective effects of *E. coli* from evolutionarily degrading
523 *M. xanthus* sporulation, possibly due to the removal of *E. coli* by nematode predation.
524

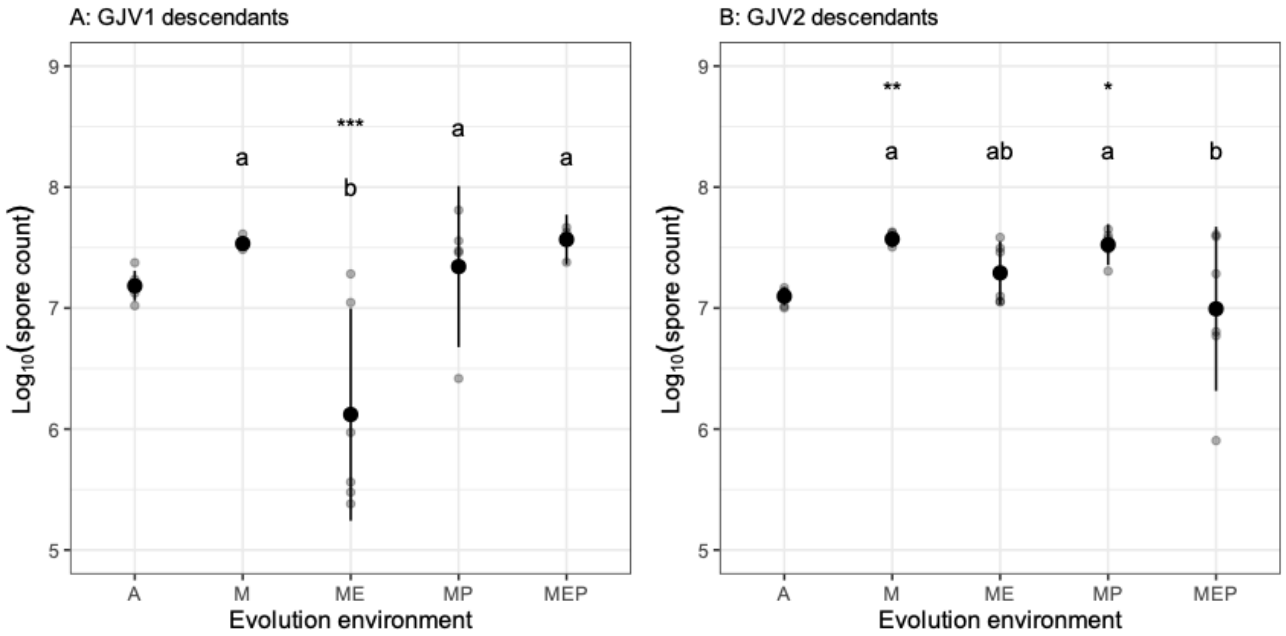

525
526

527 **Figure 6. Spore production by GJV1 and GJV2 descendants.** We counted the number of spores produced
528 on each fruiting body morphology analysis plate. Small grey dots show the mean of each evolution lineage
529 across 3-4 biological replicates, large black dots represent the mean across 4-6 replicate evolutionary
530 lineages, and blue bars show 95% confidence intervals of cross-lineage means. Asterisks indicate difference
531 from the ancestors: * = $p < 0.05$, ** = $p < 0.01$, *** = $p < 0.005$. Letters indicate statistical groups of evolution
532 treatments that do not differ within groups but differ between groups ($p < 0.05$).
533
534
535 **Discussion**
536
537 Here we characterize the phenotypic evolution of an aggregatively multicellular bacterium in
538 a multi-trophic food web, with implications for understanding the evolution of biotic networks and
539 aggregative developmental systems, including roles of historical contingency. The presence of a
540 nematode predator of *M. xanthus* strongly impacts the evolution of both *M. xanthus* fruiting body
541 morphology and spore production. *P. pacificus* had several evolutionary effects on *M. xanthus*,
542 including (i) increased fruiting-body numbers after evolution in both the absence and presence of *E.*
543 *coli* (Figure 4A; MP-vs-M and MEP-vs-ME), (ii) reduced fruiting body size, density, and density
544 heterogeneity during evolution in the absence of *E. coli* (Figure 4B-D; MP-vs-M), (iii) mitigation of
545 larger decreases in fruiting body density and density heterogeneity caused by evolution with *E. coli*
546 alone (Figure 2C,D; MEP-vs-ME, and (iv) prevention of major decreases in spore production
547 caused by evolution with *E. coli* alone (Figure 5A; MEP-vs-ME). Increased trait integration (Figure
548 S1) suggests selection on development (Pavlicev and Hansen 2011).
549
550 *Apex predation shapes aggregative developmental evolution*
551 We show that the basal prey and the apex predator in our experimental system in some
552 cases had an interacting influence on trait changes in the mesopredator. Evolution in the presence
553 of prey and absence of predators often led to the lowest values of morphological traits (Figure 4)
554 and spore production (Figure 5) (La Fortezza et al. 2022*a*). In contrast, evolution in the presence of

555 *P. pacificus* tended to lead to greater numbers of fruiting bodies relative to the ancestral phenotype
556 (Figure 4A) and contributed to a trend of increasing density and density heterogeneity compared to
557 the treatment with *E. coli* (Figure 4C-D). In the latter case, the presence of both organisms led to
558 evolution of higher trait values than the presence of *P. pacificus* alone. This could indicate an effect
559 like apparent competition between the two bacteria, where the basal prey boosts the apex
560 predator's population, increasing the apex predator's effect on the mesopredator (Holt 1977; Holt et
561 al. 1994; Holt and Bonsall 2017), or like trait-mediated indirect interactions, where pairwise species
562 interactions are altered when one or both species respond phenotypically to the presence of a third
563 (Werner and Peacor 2003). Collectively, the patterns of trait change show clear evidence of
564 evolution in response to an apex predator which affects developmental pathways in such a manner
565 that phenotypic changes emerge across different environments, in both 2- and 3-level trophic
566 communities. Here we found no evidence for faster development in MP and MEP lineages, but
567 further research into potential regulatory changes can investigate whether there are other
568 treatment-level effects on developmental timing. Studies of the ecological parameters of the
569 tripartite interaction considered here may provide insight into additional ecological drivers relevant
570 here, such as the roles of effective population size N_e in evolutionary trajectories across treatments
571 and of non-consumptive effects of predators on prey populations, behavior, and phenotypes (Sheriff
572 et al. 2020). Assessment of relative biomass of the three organisms may allow better understanding
573 of how the ecological dynamics shape the food web functioning as an ecosystem (as in (Elmhagen
574 et al. 2010)).
575
576 *Historical contingency constrains evolutionary responses to biotic selection*
577 Observations during the evolution experiment led us to test how a single mutational
578 difference between ancestral founding populations profoundly impacted *M. xanthus* evolvability in
579 response to both predator and prey. Populations which descend from GJV2, an ancestor carrying a
580 single-base-pair mutation in *rpoB*, underwent far less morphological change and diversification
581 overall than populations lacking the mutation (Figures 3, 4, & S2). A previous study found
582 differences between evolved populations descending from GJV1 and those descending from GJV2

583 in terms of colony-color evolution (Rendueles and Velicer 2017), showing additional evolutionary
584 effects of GJV2's *rpoB* allele. Single mutations have been observed to determine fitness trajectories
585 in bacteria (Aggeli et al. 2021). Our findings contribute to the growing understanding of how very
586 few genetic differences can profoundly influence how lineages respond evolutionarily to the same
587 selective conditions in unexpected ways, and relatedly, how ultimate evolutionary outcomes can be
588 contingent on small initial genetic differences (Blount et al. 2008, 2018). They also point to great
589 complexity in interplay of forces shaping the evolution of AM mesopredator systems such as *D.*
590 *dictyostelium* and *M. xanthus,* including not only who they encounter as their predators and prey,
591 but also evolutionary consequences of evolving resistance to antagonistic biotic compounds such
592 as antibiotics. The profound evolutionary consequences of this single mutation in our study may be
593 due to the mutation causing systematic differences in what adaptive pathways are followed or to
594 differences in the effects of similar adaptive pathways on the observed developmental phenotypes
595 due to epistasis (Blount et al. 2018; Aggeli et al. 2021). Alternately, the different evolutionary
596 outcomes between GJV1 and GJV2 may be due to differences in effective population size N_e, which
597 is expected to constrain evolution if within-cycle ecological dynamics reduce N_e, or to differing
598 interactions with *P. pacificus*. Further experiments should explore the ecology of this system in
599 greater detail, including carrying capacity of the three organisms, as well as the ability of *P.*
600 *pacificus* to prey on a diversity of *M. xanthus* genotypes to more fully characterize this ecological
601 interaction and to identify *M. xanthus* genes and phenotypes relevant for anti-predator defense.
602 The evolutionary effects of an antibiotic-resistance mutation we observed raise intriguing
603 questions for microbial mesopredators about possible evolutionary interactions between resisting
604 higher-order predators, resisting antibiotic-mediated antagonisms from both conspecific and
605 heterospecific microbes, and themselves preying on other microbes. It may be that resistance to
606 antibiotics which target transcription may more generally come at a cost to an organism's ability to
607 adapt to predators. Even such an aggressive (Vos and Velicer 2009; Rendueles et al. 2015;
608 Rendueles and Velicer 2017) and probably well-defended microbe as *M. xanthus* (Findlay 2016;
609 Mayrhofer et al. 2021) is likely to experience trade-offs as it deals with antagonism from competitors
610 and predators. Future research could examine potential trade-offs between competition within a

611 trophic level (*e.g.,* competition among strains or species) and selective pressure from higher trophic
612 levels, as well as the role of antibiotics and resistance to them in these conflicts (Cornforth and
613 Foster 2015).
614
615 *Ecological context and the evolution of aggregative multicellularity*
616 Because *M. xanthus* undergoes development in the abiotic selective regime used in this
617 experiment (CFcc agar), particular evolutionary changes in developmental traits may be adaptive
618 *per se.* For example, populations that evolved in the presence of *P. pacificus* may produce more
619 fruiting bodies because they evolved to form fruiting bodies faster in order to better survive
620 predation. Substantially reduced production by populations evolving with *E. coli* alone might reflect
621 relaxed selection for sporulation if *E. coli* increases the level of resources available to *M. xanthus* by
622 converting carbon sources used less efficiently *M. xanthus* into prey biomass. In this scenario, the
623 phenotypic degradation we observed in the ME treatment could be due to generic adaptation to a
624 high-resource environment (Velicer *et al.* 1998), rather than selection imposed by interactions with
625 the prey itself. Testing among hypotheses to explain specific patterns of developmental-trait
626 evolution across our treatments is of interest for future work.
627 *P. pacificus* drives the evolution of more fruiting bodies but not increased spore production
628 (Figs. 4 and 5). In fact, spore production appears to respond as an independent trait to the
629 presence of prey alone, as in La Fortezza and Velicer (La Fortezza and Velicer 2021), where spore
630 production and fruiting body morphology evolved in an uncorrelated manner. This seeming
631 independence suggests that the aggregation step of multicellular development may have evolved
632 separately from spore formation, possibly in response to predation pressures (La Fortezza et al.
633 2022*b*). This could be tested specifically by evolving a strain which is defective at fruiting body
634 formation in pure culture (Velicer et al. 2000; Schaal et al. 2022) in the presence of the predator. It
635 would also be interesting to see for how long the difference in fruiting body numbers between the M
636 and MP populations evolved here would be retained if both were to evolve further in conditions
637 without the predator. Morphological trait integration analysis indicates that evolution under
638 conditions of greater biotic complexity may support integration of *M. xanthus* developmental traits.

However, the analysis presented here is speculative and further investigation is needed, in particular into the roles of N_e and developmental constraint in this process and a potential genetic basis of trait integration.

Adaptation in predator-prey relationships spanning multiple trophic-level steps may be thought of as a process of escalation rather than one of mutual co-evolution (Vermeij 1987, 1994; Brodie and Brodie 1999). That is, changes in the morphology or behavior of a mesopredator (even for traits not directly related to predation) would drive responsive adaptation in its prey, but adaptation of the mesopredator would be driven largely by its own predators and not by the prey (Chattopadhyay and Dutta 2013; Klompmaker et al. 2017). A previous study has shown that prey identity can strongly affect how *M. xanthus* fruiting body phenotypes evolve indirectly (La Fortezza et al. 2022*a*) but in that study the prey did not co-evolve with *M. xanthus* (as also in this study), and fruiting body formation was not under direct selection. A subsequent evolution experiment would be of interest to test whether prey presence and type affect *mesopredator* AM evolution when an apex predator is present and when all parties can freely co-evolve, as well as to examine relative effects of the apex predator and basal prey.

How predation and multicellular development relate to each other in the evolutionary history of the myxobacteria is not yet well understood. Future comprehensive identification and phylogenetic analysis of the genes involved in both behaviors will improve understanding of their relative origins. While many selective forces are likely shape the evolution and diversification of aggregative multicellular systems (Bonner 1998; La Fortezza et al. 2022*b*), our results point to not only predation by mesopredators, but also predation on them, playing important roles.

Literature Cited

Abrams, P. A. 2000. The Evolution of Predator-Prey Interactions: Theory and Evidence. Annual Review of Ecology and Systematics 31:79–105.

Aggeli, D., Y. Li, and G. Sherlock. 2021. Changes in the distribution of fitness effects and adaptive mutational spectra following a single first step towards adaptation. Nature Communications 12.

Blount, Z. D., C. Z. Borland, and R. E. Lenski. 2008. Historical contingency and the evolution of a key innovation in an experimental population of *Escherichia coli*. Proceedings of the National Academy of Sciences 105:7899–7906.
Blount, Z. D., R. E. Lenski, and J. B. Losos. 2018. Contingency and determinism in evolution: Replaying life's tape. Science 362.
Bonner, J. T. 1998. The origins of multicellularity. Integrative Biology: Issues, News, and Reviews 1:27–36.
———. 2009. The Social Amoebae: The Biology of Cellular Slime Molds. Princeton University Press, Princeton.
Boraas, M. E., D. B. Seale, and J. E. Boxhorn. 1998. Phagotrophy by flagellate selects for colonial prey: A possible origin of multicellularity. Evolutionary Ecology 12:153–164.
Brenner, S. 1974. The genetics of *Caenorhabditis elegans*. Genetics 77:71–94.
Bretscher, A. P., and D. Kaiser. 1978. Nutrition of *Myxococcus xanthus*, a Fuiting Myxobacterium. Journal of Bacteriology 133:763–768.
Brodie, E. D., and E. D. Brodie. 1999. Predator-Prey Arms Races. BioScience 49:557–568.
Bull, C. T., K. G. Shetty, and K. V. Subbarao. 2002. Interactions between myxobacteria, plant pathogenic fungi, and biocontrol agents. Plant Disease 86:889–896.
Chattopadhyay, D., and S. Dutta. 2013. Prey selection by drilling predators: A case study from Miocene of Kutch, India. Palaeogeography, Palaeoclimatology, Palaeoecology 374:187–196.
Claessen, D., D. E. Rozen, O. P. Kuipers, L. Søgaard-Andersen, and G. P. van Wezel. 2014. Bacterial solutions to multicellularity: a tale of biofilms, filaments and fruiting bodies. Nature Reviews Microbiology 12:115–124.
Cornforth, D. M., and K. R. Foster. 2015. Antibiotics and the art of bacterial war. Proceedings of the National Academy of Sciences of the United States of America 112:10827–10828.
Dahl, J. L., C. H. Ulrich, and T. L. Kroft. 2011. Role of phase variation in the resistance of *Myxococcus xanthus* fruiting bodies to *Caenorhabditis elegans* predation. Journal of Bacteriology 193:5081–5089.
DePas, W. H., A. K. Syed, M. Sifuentes, J. S. Lee, D. Warshaw, V. Saggar, G. Csankovszki, et al. 2014. Biofilm formation protects *Escherichia coli* against killing by *Caenorhabditis elegans* and *Myxococcus xanthus*. Applied and Environmental Microbiology 80:7079–7087.
Elmhagen, B., G. Ludwig, S. P. Rushton, P. Helle, and H. Linden. 2010. Top predators, mesopredators and their prey: interference ecosystems along bioclimatic productivity gradients. Journal of Animal Ecology 79:785–794.
Findlay, B. L. 2016. The Chemical Ecology of Predatory Soil Bacteria. ACS Chemical Biology 11:1502–1510.
Grosberg, R. K., and R. R. Strathmann. 2007. The Evolution of Multicellularity: A Minor Major Transition? Annual Review of Ecology, Evolution, and Systematics 38:621–654.
Herron, M., P. Conlin, and W. Ratcliff, eds. 2022. The Evolution of Multicellularity. Evolutionary Cell Biology (1st ed.). CRC Press, Boca Raton.
Herron, M. D. 2016. Origins of multicellular complexity: *Volvox* and the volvocine algae. Molecular Ecology 25:1213–1223.
Herron, M. D., J. M. Borin, J. C. Boswell, J. Walker, I.-C. K. Chen, C. A. Knox, M. Boyd, et al. 2019. De novo origins of multicellularity in response to predation. Scientific Reports 9:2328.
Hillesland, K. L., G. J. Velicer, and R. E. Lenski. 2009. Experimental evolution of a microbial predator's ability to find prey. Proceedings of the Royal Society B: Biological Sciences 276:459–67.
Holt, R. D. 1977. Predation, apparent competition, and the structure of prey communities. Theoretical Population Biology 12:197–229.
Holt, R. D., and M. B. Bonsall. 2017. Apparent Competition. Annual Review of Ecology, Evolution, and Systematics 48:447–471.
Holt, R. D., J. Grover, and D. Tilman. 1994. Simple Rules for Interspecific Dominance in Systems with Exploitative and Apparent Competition. The American Naturalist 144:741–771.
Hong, R. L., and R. J. Sommer. 2006. *Pristionchus pacificus*: A well-rounded nematode. BioEssays 28:651–659.
Isaksson, H., P. Lind, and E. Libby. 2025. Adaptive evolutionary trajectories in complexity: Transitions between unicellularity and facultative differentiated multicellularity. Proceedings of the National Academy of Sciences 122:e2411692122.
Jahan, I., T. J. Scott, J. E. Strassmann, and D. C. Queller. 2025. Testing the coordination hypothesis: incompatibilities in aggregative development of an experimentally evolved social amoeba. Evolution Letters 9:236–248.
Kapsetaki, S. E., R. M. Fisher, and S. A. West. 2016. Predation and the formation of multicellular groups in algae. Evolutionary Ecology Research 17:651–669.
Kauffman, A., L. Parsons, G. Stein, A. Wills, R. Kaletsky, and C. Murphy. 2011. *C. elegans* positive butanone learning, short-term, and long-term associative memory assays. Journal of Visualized Experiments 1–10.

Kessin, R. H., G. G. Gundersen, V. Zaydfudim, M. Grimson, and R. L. Blanton. 1996. How cellular slime molds evade nematodes. Proceedings of the National Academy of Sciences of the United States of America 93:4857–4861.

Klompmaker, A. A., M. Kowalewski, J. W. Huntley, and S. Finnegan. 2017. Increase in predator-prey size ratios throughout the Phanerozoic history of marine ecosystems. Science 356:1178–1180.

Kreth, J., J. W. Lengeler, and K. Jahreis. 2013. Characterization of Pyruvate Uptake in Escherichia coli K-12. PLOS ONE 8.

Kroos, L. 2017. Highly Signal-Responsive Gene Regulatory Network Governing *Myxococcus* Development. Trends in Genetics 33:3–15.

Kroos, L., D. Wall, J. Muñoz-Dorado, P. I. Higgs, M. Singer, S. T. Islam, E. M. F. Mauriello, et al. 2025. Milestones in the development of *Myxococcus xanthus* as a model multicellular bacterium. Journal of Bacteriology (accepted).

La Fortezza, M., O. Rendueles, H. Keller, and G. J. Velicer. 2022*a*. Hidden paths to endless forms most wonderful: ecology latently shapes evolution of multicellular development in predatory bacteria. Communications Biology 5:977.

La Fortezza, M., K. A. Schaal, and G. J. Velicer. 2022*b*. Group Formation: On the Evolution of Aggregative Multicellularity. Pages 89–110 *in* M. D. Herron, P. L. Conlin, and W. C. Ratcliff, eds. The Evolution of Multicellularity. CRC Press, Boca Raton.

La Fortezza, M., and G. J. Velicer. 2021. Social selection within aggregative multicellular development drives morphological evolution. Proceedings of the Royal Society B 288.

Livingstone, P. G., R. M. Morphew, and D. E. Whitworth. 2017. Myxobacteria are able to prey broadly upon clinically-relevant pathogens, exhibiting a prey range which cannot be explained by phylogeny. Frontiers in Microbiology 8:1–9.

Machado, F. A., A. Hubbe, D. Melo, A. Porto, and G. Marroig. 2019. Measuring the magnitude of morphological integration: The effect of differences in morphometric representations and the inclusion of size. Evolution 73:2518–2528.

Manhes, P., and G. J. Velicer. 2011. Experimental evolution of selfish policing in social bacteria. Proceedings of the National Academy of Sciences 108:8357–8362.

Márquez-Zacarías, P., P. L. Conlin, K. Tong, J. T. Pentz, and W. C. Ratcliff. 2021. Why have aggregative multicellular organisms stayed simple? Current Genetics 67:871–876.

Mayrhofer, N., G. J. Velicer, K. A. Schaal, and M. Vasse. 2021. Behavioral Interactions between Bacterivorous Nematodes and Predatory Bacteria in a Synthetic Community. Microorganisms 9:1362.

Melo, D., G. Garcia, A. Hubbe, A. P. Assis, and G. Marroig. 2016. EvolQG - An R package for evolutionary quantitative genetics [version 3; referees: 2 approved, 1 approved with reservations]. F1000Research 4.

Mendes-Soares, H., and G. J. Velicer. 2013. Decomposing Predation: Testing for Parameters that Correlate with Predatory Performance by a Social Bacterium. Microbial Ecology 65:415–23.

Morgan, A. D., R. C. MacLean, K. L. Hillesland, and G. J. Velicer. 2010. Comparative Analysis of *Myxococcus* Predation on Soil Bacteria. Applied and Environmental Microbiology 76:6920–6927.

Müller, S., S. N. Strack, S. E. Ryan, D. B. Kearns, and J. R. Kirby. 2015. Predation by *Myxococcus xanthus* induces *Bacillus subtilis* to form spore-filled megastructures. Applied and Environmental Microbiology 81:203–210.

Nair, R. R., M. Vasse, S. Wielgoss, L. Sun, Y.-T. N. Yu, and G. J. Velicer. 2019. Bacterial predator-prey coevolution accelerates genome evolution and selects on virulence-associated prey defences. Nature Communications 10:4301.

Nair, R. R., and G. J. Velicer. 2021. Predatory bacteria select for sustained prey diversity. Microorganisms 9:1–14.

Oksanen, J., F. G. Blanchet, M. Friendly, R. Kindt, P. Legendre, D. McGlinn, P. R. Minchin, et al. 2020. vegan: Community Ecology Package.

Pavlicev, M., J. M. Cheverud, and G. P. Wagner. 2009. Measuring Morphological Integration Using Eigenvalue Variance. Evolutionary Biology 36:157–170.

Pavlicev, M., and T. F. Hansen. 2011. Genotype-Phenotype Maps Maximizing Evolvability: Modularity Revisited. Evolutionary Biology 38:371–389.

Pentz, J. T., T. Limberg, N. Beermann, and W. C. Ratcliff. 2015. Predator Escape: An Ecologically Realistic Scenario for the Evolutionary Origins of Multicellularity. Evolution: Education and Outreach 8:13.

Pentz, J. T., P. Márquez-Zacarías, G. O. Bozdag, A. Burnetti, P. J. Yunker, E. Libby, and W. C. Ratcliff. 2020. Ecological Advantages and Evolutionary Limitations of Aggregative Multicellular Development. Current Biology 30:4155-4164.e6.

Pérez, J., J. Munoz-Dorado, A. F. Brana, L. J. Shimkets, L. Sevillano, and R. I. Santamaría. 2011. *Myxococcus xanthus* induces actinorhodin overproduction and aerial mycelium formation by *Streptomyces coelicolor*. Microbial Biotechnology 4:175–183.

Pires da Silva, A. 2013. *Pristionchus pacificus* protocols. WormBook 1–20.
R Core Team. 2024. R: A language and environment for statistical computing. R Foundation for Statistical Computing, Vienna, Austria.
Ratcliff, W. C., R. F. Denison, M. Borrello, and M. Travisano. 2012. Experimental evolution of multicellularity. Proceedings of the National Academy of Sciences 109:1595–1600.
Rendueles, O., and G. J. Velicer. 2017. Evolution by flight and fight: diverse mechanisms of adaptation by actively motile microbes. The ISME Journal 11:555–568.
Rendueles, O., P. C. Zee, I. Dinkelacker, M. Amherd, S. Wielgoss, and G. J. Velicer. 2015. Rapid and widespread de novo evolution of kin discrimination. Proceedings of the National Academy of Sciences 112:9076–9081.
Rivera-Yoshida, N., A. V. Arzola, J. A. Arias Del Angel, A. Franci, M. Travisano, A. E. Escalante, and M. Benítez. 2019. Plastic multicellular development of *Myxococcus xanthus* : genotype–environment interactions in a physical gradient. Royal Society Open Science 6:181730.
RStudio Team. 2020. RStudio: Integrated Development for R. RStudio, PBC, Boston, MA.
Schaal, K. A., Y.-T. Nicco Yu, M. Vasse, and G. J. Velicer. 2022. Allopatric divergence of cooperators confers cheating resistance and limits the effects of a defector mutation. bioRxiv 2021.01.07.425765.
Schindelin, J., I. Arganda-Carreras, E. Frise, V. Kaynig, M. Longair, T. Pietzsch, S. Preibisch, et al. 2012. Fiji: An open-source platform for biological-image analysis. Nature Methods 9:676–682.
Sheriff, M. J., S. D. Peacor, D. Hawlena, and M. Thaker. 2020. Non-consumptive predator effects on prey population size: A dearth of evidence. (J. Gaillard, ed.)Journal of Animal Ecology 89:1302–1316.
Shimkets, L. J., M. Dworkin, and H. Reichenbach. 2006*a*. The Myxobacteria. Pages 31–115 *in*The Prokaryotes. Springer New York, New York, NY.
Shimkets, L. J., M. Dworkin, and H. Reichenbach. 2006*b*. The Myxobacteria. Prokaryotes.
Stanley, S. M. 1973. An Ecological Theory for the Sudden Origin of Multicellular Life in the Late Precambrian. Proceedings of the National Academy of Sciences 70:1486–1489.
Stiernagle, T. 2006. Maintenance of *C. elegans*. Pages 1–11 *in*WormBook. The C. elegans Research Community, WormBook.
Urban, M. C. 2013. Evolution mediates the effects of apex predation on aquatic food webs. Proceedings of the Royal Society B: Biological Sciences 280:20130859.
Velicer, G. J., L. Freund, M. La Fortezza, N. Mayrhofer, and K. A. Schaal. 2024. MyxoEE.
Velicer, G. J., L. Kroos, and R. E. Lenski. 1998. Loss of social behaviors by *Myxococcus xanthus* during evolution in an unstructured habitat. Proceedings of the National Academy of Sciences 95:12376–12380.
Velicer, G. J., L. Kroos, and R. E. Lenski. 2000. Developmental cheating in the social bacterium *Myxococcus xanthus*. Nature 404:598–601.
Velicer, G. J., R. E. Lenski, and L. Kroos. 2002. Rescue of social motility lost during evolution of *Myxococcus xanthus* in an asocial environment. Journal of Bacteriology 184:2719–2727.
Velicer, G. J., G. Raddatz, H. Keller, S. Deiss, C. Lanz, I. Dinkelacker, and S. C. Schuster. 2006. Comprehensive mutation identification in an evolved bacterial cooperator and its cheating ancestor. Proceedings of the National Academy of Sciences 103:8107–8112.
Velicer, G. J., and M. Vos. 2009. Sociobiology of the Myxobacteria. Annual Review of Microbiology 63:599–623.
Vermeij, G. J. 1987. Evolution and Escalation: An Ecological History of Life. Princeton University Press.
———. 1994. THE EVOLUTIONARY INTERACTION AMONG SPECIES: Selection, Escalation, and Coevolution. Annual Review of Ecology and Systematics 25:219–236.
Vos, M., and G. J. Velicer. 2009. Social Conflict in Centimeter-and Global-Scale Populations of the Bacterium *Myxococcus xanthus*. Current Biology 19:1763–1767.
Werner, E. E., and S. D. Peacor. 2003. A review of trait-mediated indirect interactions in ecological communities. Ecology 84:1083–1100.
Wickham, H. 2016. ggplot2: Elegant Graphics for Data Analysis. Springer-Verlag New York.
Zee, P. C., H. Mendes-Soares, Y.-T. N. Yu, S. A. Kraemer, H. Keller, S. Ossowski, K. Schneeberger, et al. 2014. A shift from magnitude to sign epistasis during adaptive evolution of a bacterial social trait. Evolution 68:2701–2708.